Journal of Quantitative Spectroscopy & Radiative Transfer 262 (2021) 107517

Contents lists available at ScienceDirect

Journal of Quantitative Spectroscopy & Radiative Transfer

journal homepage: www.elsevier.com/locate/jqsrt

First high-resolution analysis of the $3\nu_4$, $\nu_2+2\nu_4$ and $2\nu_2+\nu_4$ bands of $^{76}GeH_4$

O.N. Ulenikov[a,*], O.V. Gromova[a], E.S. Bekhtereva[a], N.I. Raspopova[a], I.A. Velmuzhova[b], M.A. Koshelev[c], P.G. Sennikov[b]

[a] Research School of High-Energy Physics, National Research Tomsk Polytechnic University, Tomsk 634050, Russia
[b] G.G. Devyatykh Institute of Chemistry of High Purity Substances, Russian Academy of Sciences, Nizhny Novgorod 603950, Russia
[c] Institute of Applied Physics, Russian Academy of Sciences, Nizhny Novgorod 603950, Russia

ARTICLE INFO

Article history:
Received 14 December 2020
Revised 9 January 2021
Accepted 9 January 2021
Available online 13 January 2021

Keywords:
The $3\nu4/\nu2+2\nu4/2\nu2+\nu4$ interacting states of GeH4
resonance interactions in spherical top molecules
determination of spectroscopic parameters

ABSTRACT

The infrared spectrum of germane, purified and enriched up to 88.1% of $^{76}GeH_4$, was measured at the temperature of $(22.6\pm0.1)\,^{\circ}C$ with a Bruker Fourier transform infrared spectrometer IFS125HR and analyzed in the region of 2350–2730 cm^{-1} where the bending tetrad of the ro-vibrational octad of germane is located. The 2955 transitions belonging to the thirteen sub-bands of the Tetrad were assigned and theoretically analysed in the frame of the effective Hamiltonian model. The obtained set of 98 fitted parameters reproduces the initial 2955 experimental line positions with the $d_{rms}=6.43\times10^{-4}$ cm^{-1}. A list of assigned experimental transitions is presented as the Supplementary material to the present paper.

1. Introduction

Knowledge of internal properties of the germane molecule is very important for numerous both pure scientific and applied problems of physics, chemistry, astrophysics, industry, etc. Germane in a trace amount can be found in the space [1] and as one of the components of atmospheres of giant gas-planet such as Jupiter and Saturn, Corice et al. [2], Fink et al. [3], Kunde et al. [4], Drossart et al. [5], Chen et al. [6], Atreya et al. [7], Lodders [8], and its presence should be taken into account in studies of the compositions and chemistry of their atmospheres. In particular, in the atmospheres of Jupiter and Saturn germane was detected at abundances orders of magnitude higher than their thermochemical equilibrium concentrations in the upper troposphere [9]. Germane in a natural isotopic composition is used for producing high-purity germanium. On that basis various physical devices (e.g., high-sensitivity detectors of nuclear radiation) are manufactured [10]. Germane enriched by ^{76}Ge up to 88% can be used as a starting substance for the production of high purity single-crystal ^{76}Ge which, can be applied as a source of double beta decay of its nuclei and, at the same time, as a detector of this process [11]. In physical chemistry, germane as well as silane can be considered as a prototype of numerous organoequivalent molecules [12,13]. One of the important problems in chemical physics is the precise determination of the intramolecular multidimensional potential and dipole moment surfaces, which can be exploited in numerous applied investigations. This problem can be solved by semi-empirical methods, Thyagarajan et al. [14], Bekhtereva et al. [15], or on the basis of *ab initio* calculations (see, e.g., [16]). In both cases, the knowledge of highly accurate spectroscopic information not only on the main species, but also on all possible isotopologues is important. Because of these reasons the germane molecule has been extensively studied for many years (see, Corice et al. [17], Kattenberg et al. [18], Ozier and Rosenberg [19], Lepage et al. [20], Kreiner et al. [21], [22], Daunt et al. [23], Corice [24], Kagann et al. [25], Fox et al. [26], Kreiner et al. [27], Magerl et al. [28], Kreiner et al. [29], Lepage et al. [30], Das et al. [31], Schaeffer and Lovejoy [32], Cadot [33], Varanasi and Chudamani [34], Zhu et al. [35], Halonen [36], Zhu and Thrush [37], Zhu et al. [38], Campargue et al. [39], Zhu et al. [40], Sun et al. [41], Chen et al. [42], Boudon et al. [43], Richard et al. [44] and references therein).

Germane in a natural isotopic composition produces complex infrared spectra, at least as five stable isotopologues exist in proper abundances with the mass numbers 70 (20.55%), 72 (27.37%), 73 (7.67%), 74 (36.74%), and 76 (7.67%). Additional complexity of the germane spectra arises from very strong Coriolis interaction between pairs of its fundamentals, ν_2/ν_4 and ν_1/ν_3. Germane is a spherical top molecule. It has no permanent dipole moment, and

* Corresponding author.
E-mail address: Ulenikov@mail.ru (O.N. Ulenikov).

https://doi.org/10.1016/j.jqsrt.2021.107517
0022-4073/

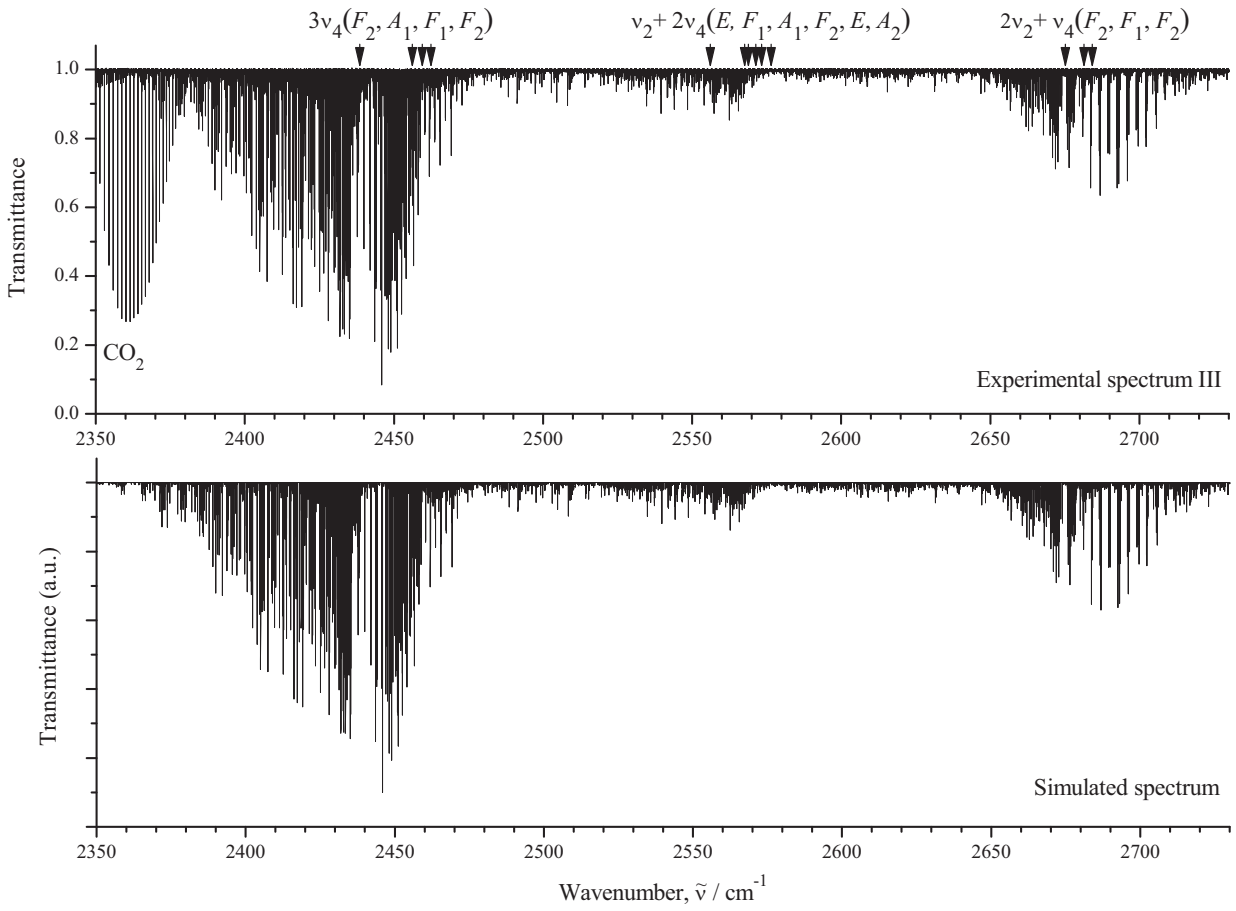

Fig. 1. Overview spectrum III of $^{76}GeH_4$ enriched up to 88.1 % (upper trace) in the region of 2350–2730 cm^{-1} (for the experimental conditions, see Section 2). Band centra of the $3\nu_4$, $\nu_2+2\nu_4$ and $2\nu_2+\nu_4$ bands of $^{76}GeH_4$ are marked. The bottom trace present corresponding simulated spectrum (see text for the conditions of the simulation).

the particularities of $k-l$-splittings in such molecules lead to only one strong transition for any component of the $k-l$ triplet (all other transitions are considerably weaker), see, e.g., [45,46]. As a consequence, the use of the ground state combination differences method which is efficient for the study of molecules of different type (see, e.g., Refs. [47–52]) is very limited as applied to germane, and the assignment of transitions in infrared spectra of this molecule is not a simple problem.

In the present work we focus on the study of the octad bending tetrad vibrational bands of the $^{76}GeH_4$ specially enriched species which, to our knowledge, was not analysed before. The use of enriched sample made it possible for us to significantly reduce difficulties in the spectrum analyzing connecting with the the need to take into account the presence of other germane isotopologues in the spectrum.

2. Experimental

The enriched and purified gas sample of germane containing $^{76}GeH_4$ (88.1%), $^{74}GeH_4$ (11.5%), $^{73}GeH_4$ (0.07%), $^{72}GeH_4$ (0.17%), and $^{70}GeH_4$ (0.12%) isotopologues was spectroscopically studied using a Bruker IFS125HR Fourier transform spectrometer. The experimental details are presented in Table 1. Briefly, the spectrometer was equipped with a Globar source, a KBr beam splitter and a liquid nitrogen cooled indium antimonide (InSb) detector. The sample spectra were recorded with high resolution of 0.003 cm^{-1} (the resolution due to the maximum optical path difference) in the frequency range 1800–4500 cm^{-1}. The aperture size was 1 mm. The Norton–Beer (weak) apodization function was applied. A multi-pass White cell was permanently connected to the vacuum system with a gas sample vacuum system, a turbo-molecular pump, and capacitance pressure gauges covering the 10^{-3}–100 Torr range. The optical compartment of the spectrometer was evacuated by a mechanical pump down to 0.02 Torr (or less) and that pressure remained during the experiment.

The final spectra (see Fig. 1) were obtained by averaging about 1000 co-added scans. In total, three spectra were recorded at two different optical path lengths (0.75 m and 3.75 m) and three different pressures, 0.3 Torr, 1.5 Torr and 3 Torr (spectrum I, II and III, respectively), to cover a wider range of J numbers. The final spectra were calibrated using most intense and well resolved lines of H_2O, CO_2 and HITRAN database line list [53]. After calibration the standard deviation of the difference between the measured and tabulated peak positions was estimated to be about 2×10^{-4} cm^{-1}. Comparison of the positions of unsaturated unblended lines in different experimental spectra shown their agreement within $\pm10^{-4}$, which demonstrates a negligible effect of the pressure shift and good data precision.

3. Brief theoretical background

Germane is a spherical top molecule which symmetry group is isomorphic to the T_d point symmetry group. This molecule has a tetrahedral structure resulting in one nondegenerate (q_1, A_1), one doubly degenerate (q_2, E), and two triply degenerate (q_3, F_2) and (q_4, F_2) vibrational modes. It is well known (see, e.g., Refs. [54–56]) that ro-vibrational states of such molecules are divided into groups (polyads) of more or less isolated states which interact with each

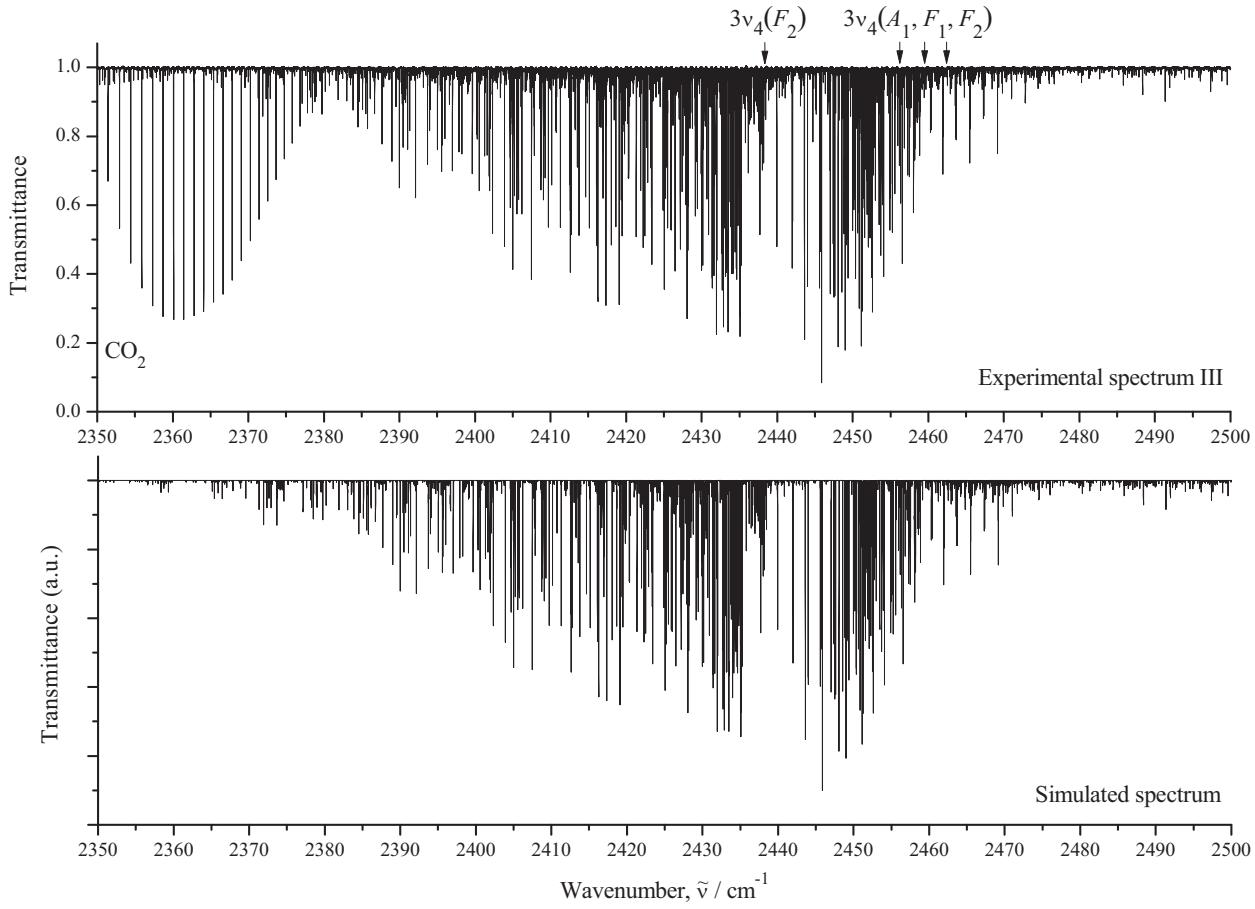

Fig. 2. More in detail overview spectrum III of $^{76}GeH_4$ in the region of the $3\nu_4$ band (for the experimental conditions, see Section 2). The bottom trace present corresponding simulated spectrum (see text for conditions of the simulation).

Table 1
Experimental setup for the regions 1800–4500 cm^{-1} of the infrared spectrum of $^{M}GeH_4$ ($M = 76, 74$).

Spectr.	Resolution/cm^{-1}	Measuring time/h	No. of scans	Source	Detector	Beam splitter	Opt. path length/m	Aperture/mm	Temp. /°C	Pressure/Torr	Calibr. gas
I	0.003	40.2	1200	Globar	InSb	KBr	3.75	1.0	22.7	0.3	H_2O, CO_2
II	0.003	36.9	1100	Globar	InSb	KBr	0.75	1.0	28.8	1.5	H_2O, CO_2
III	0.003	35.2	1050	Globar	InSb	KBr	3.75	1.0	22.6	3.0	H_2O, CO_2

other inside of a polyad. In the present paper we deal with the tetrad of the $3\nu_4$, $\nu_2 + 2\nu_4$, $2\nu_2 + \nu_4$ and $3\nu_2$ bending bands (sixteen ro-vibrational sub-bands) of the so-called Octad of the $^{76}GeH_4$ molecule. We note that in the present paper we were not able to assign transitions to the extremely very weak $3\nu_2$ band, and, for this reason, the latter band was considered in the present work as a "dark"band which, in spite of the absence of transitions taken into account, effects on the ro-vibrational structure of the considered $3\nu_4$, $\nu_2 + 2\nu_4$ and $2\nu_2 + \nu_4$ bands because of the presence of resonance interactions. On the other hand, the tetrad of the bending state is not strongly coupled with the four $\nu_1 + \nu_2$, $\nu_1 + \nu_4$, $\nu_2 + \nu_3$ and $\nu_3 + \nu_4$ stretching bands of octad, and for this reason, we did not take stretching bands into account.

The high symmetry of the GeH_4 molecule requires using a special mathematical formalism: the theory of Irreducible Tensorial Sets (see, e.g., Refs. [57–61]) for the description of its spectra. Application of the mentioned formalism to the XY_4 (T_d) molecules has been discussed in the spectroscopic literature many times (see, e.g., Refs. [62–66]). For that reason we present only briefly the main points necessary for understanding the procedure of calculations with the effective Hamiltonian of the XY_4 spherical top molecule.

As is known from general vibration-rotation theory [67–69], the Hamiltonian of an arbitrary polyatomic molecule can be reduced to a set of the so-called effective Hamiltonians, or, in a more general case, to a set of effective operator matrices of the form (it was discussed in the literature many times, see, e.g., [70–74])

$$H^{vib.-rot.} = \sum_{a,b} |a\rangle\langle b| H^{a,b}, \quad (1)$$

where $|a\rangle$ and $\langle b|$ are the basic vibrational functions; the operators $H^{a,b}$ depend on the rotational operators J_α ($\alpha = x, y, z$) only, and summation is performed on all degenerate and/or interacting vibrational states. When, as in our case, a molecule possesses a

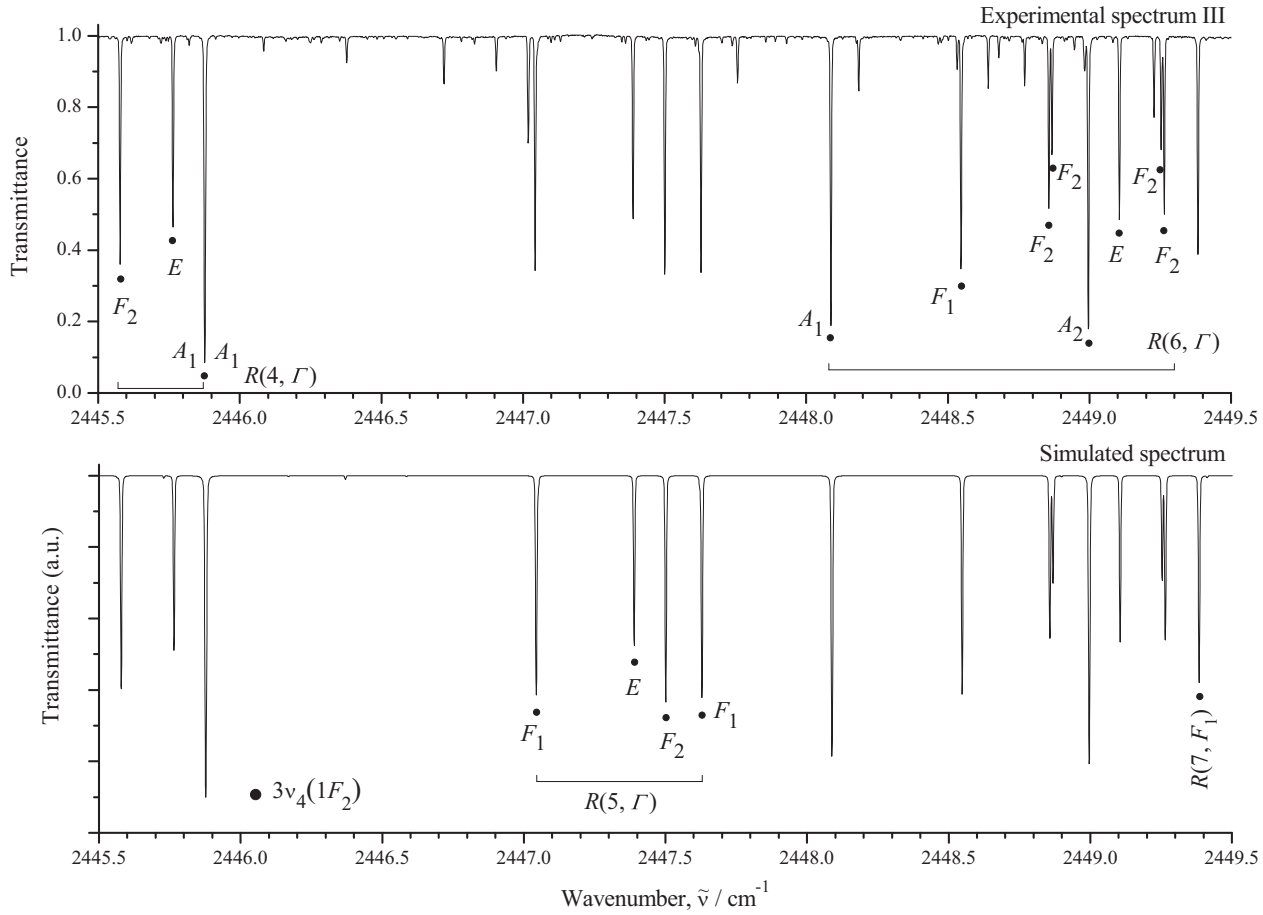

Fig. 3. Small part of the high resolution experimental spectrum III of $^{76}GeH_4$ in the region of the R-branch of the $3\nu_4$ band (top trace). Bottom trace shows the corresponding simulated spectrum lines of the $3\nu_4, 1F_2$ band are marked by dark circles.

symmetry, Eq. (1) can be rewritten in the symmetrized form [61]:

$$H^{vib.-rot.} = \sum_{\nu\gamma,\nu'\gamma'} \sum_{n\Gamma} [(|\nu\gamma\rangle \otimes \langle\nu'\gamma'|)^{n\Gamma} \otimes H^{n\Gamma}_{\nu\gamma,\nu'\gamma'}]^{A_1} \equiv \sum_{\nu\gamma,\nu'\gamma'} \sum_{n\Gamma} \sum_{\Omega K} [(|\nu\gamma\rangle \otimes \langle\nu'\gamma'|)^{n\Gamma} \otimes R^{\Omega(K,n\Gamma)}]^{A_1} Y^{\Omega(K,n\Gamma)}_{\nu\gamma,\nu'\gamma'}. \quad (2)$$

In Eq. (2):

(a). $|\nu\gamma\rangle$ are the symmetrized vibrational functions, γ are symmetries of these functions; $R^{\Omega(K,n\Gamma)}_{\sigma}$ are symmetrized rotational operators, and Ω is the total degree of the rotational operators J_α in the individual operator R; K is the rank of this operator (see, e.g., [75]), Γ is its symmetry in the T_d point symmetry group, and n distinguishes between different possible operators $R^{\Omega(K,n\Gamma)}_{\sigma}$ having the same values of Ω, K and Γ. The sign $\otimes$ denotes a tensorial product, and the values $Y^{\Omega(K,n\Gamma)}_{\nu\gamma,\nu'\gamma'}$ are different-type spectroscopic parameters.

(b). The symmetrized rotational operators, $R^{\Omega(K,n\Gamma)}_{\sigma}$, are determined as, Zhilinskii [75]),

$$R^{\Omega(K,n\Gamma)}_{\sigma} = \sum_{m} {}^{(K)}G^{m}_{n\Gamma\sigma} R^{\Omega(K)}_{m}, \quad (3)$$

where the rotational operators $R^{\Omega(K)}_{m}$ are symmetrized in the SO(3) symmetry group and can be constructed in accordance with the recurrence relation, Cheglokov et al. [66], Zhilinskii [75]:

$$R^{\Omega+1(K+1)}_{\tilde{m}} = \sum_{l=-1,0,1} C^{K+1\ \tilde{m}}_{K\ \tilde{m}-l,1\ l} R^{\Omega(K)}_{\tilde{m}-l} R^{1(1)}_{l}, \quad (4)$$

where $C^{K+1\ \tilde{m}}_{K\ \tilde{m}-l,1\ l}$ are known Clebsh–Gordan coefficients, Ref. [59]. The irreducible rotational operators $R^{\Omega(K)}_{m}$ with $K < \Omega$ (in this case, the parity of both Ω and K must be the same, Zhilinskii [75]) are constructed as,

$$R^{\Omega(K)}_{m} = R^{\Omega=K(K)}_{m} (R^{2(0)})^{(\Omega-K)/2}, \quad (5)$$

where the notation $R^{2(0)} = (J^2_x + J^2_y + J^2_z)$ is used. In this case, the tensorial components of the first order operator $R^{1(1)}_{m}$ $(m = 0, \pm 1)$ are determined as

$$R^{1(1)}_{1} = -\frac{1}{\sqrt{2}}(J_x - iJ_y) \equiv -J_+,$$
$$R^{1(1)}_{-1} = \frac{1}{\sqrt{2}}(J_x + iJ_y) \equiv J_-,$$
$$R^{1(1)}_{0} = J_z \equiv J_0, \quad (6)$$

where

$$J_x = i\frac{\cos\varphi}{\sin\theta}\left(\frac{\partial}{\partial\psi} - \cos\theta\frac{\partial}{\partial\varphi}\right) - i\sin\varphi\frac{\partial}{\partial\theta},$$
$$J_y = -i\frac{\sin\varphi}{\sin\theta}\left(\frac{\partial}{\partial\psi} - \cos\theta\frac{\partial}{\partial\varphi}\right) - i\cos\varphi\frac{\partial}{\partial\theta}, \quad (7)$$

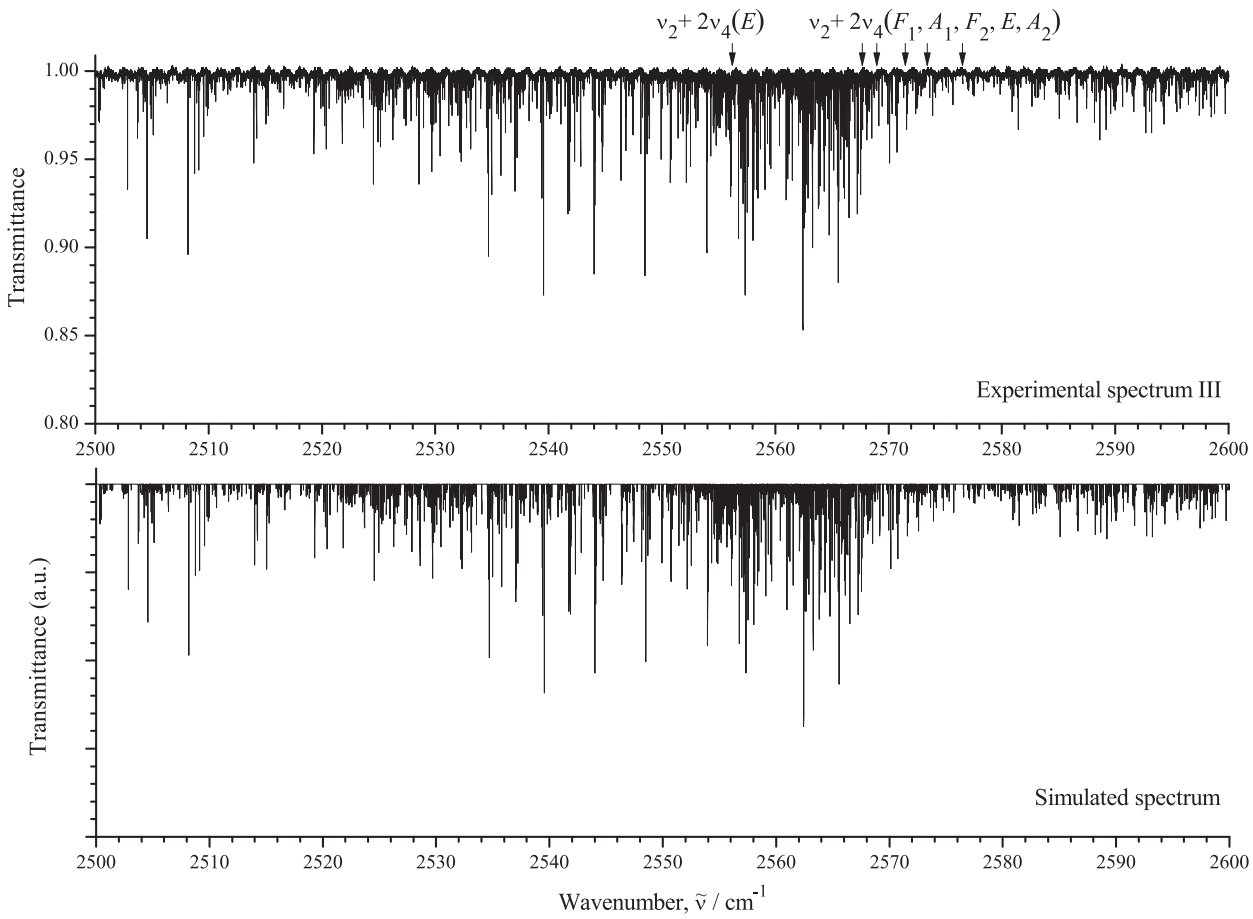

Fig. 4. More in detail overview spectrum III of $^{76}GeH_4$ in the region of the $\nu_2 + 2\nu_4$ band (for the experimental conditions, see Section 2). The bottom trace present corresponding simulated spectrum (see text for the conditions of the simulation).

and

$$J_z = -i\frac{\partial}{\partial\varphi}. \tag{8}$$

The values ${}^{(K)}G^{m}_{n\Gamma\sigma}$, Eq. (3), of the orientation matrix G can be found in the literature (see, e.g., Champion [64], Moret-Bailly et al. [76], Rey et al. [77]).

4. Description of the spectra and assignment of transitions

The upper part of Fig. 1 presents the survey spectrum III of $^{76}GeH_4$ in the region of 2350–2730 cm^{-1}. One can see three pronounced bands of the bending tetrad with the labeling of sub-bands. To give the reader more impression about quality of the recorded spectra, three pairs of Figs. 2–7 present both the low resolution spectra in regions of separate banding bands of the GeH_4 octad and small parts of high resolution spectra in corresponding spectral regions. One can see clearly pronounced rotational cluster structures in Figs. 2–7. At the same time, as can be seen from Figs. 4 and 5, cluster structures are absent in sub-bands of the $\nu_2 + 2\nu_4$ band.

As was mentioned above, the GeH_4 molecule is a spherical top with a symmetry group isomorphic to the T_d point symmetry group. As a consequence, transitions in absorption are allowed only between vibrational states $(v\Gamma)$ and $(v'\Gamma')$ for which the relation (see, e.g., [78])

$$\Gamma \otimes \Gamma' \ni F_2 \tag{9}$$

is fulfilled. As a consequence, five sub-bands of the F_2 symmetry $((3\nu_4; 1F_2, 2F_2)$, $(\nu_2 + 2\nu_4; F_2)$ and $(2\nu_2 + \nu_4; 1F_2, 2F_2))$ of the thirteen sub-bands of the three bending bands, $3\nu_4$, $\nu_2 + 2\nu_4$ and $2\nu_2 + \nu_4$, of the Tetrad are allowed in absorption by the symmetry of the GeH_4 molecule. All the other eight bands are forbidden in absorption by the symmetry, but in our analysis transitions belonging to five of them (see Table 2 for detail) have been assigned because of the presence of strong Coriolis-type interactions between the states of the bending Tetrad and borrowing intensity by the "forbidden"sub-bands from the "allowed" ones.

Assignment of transitions was performed simultaneously with the fit of values of spectroscopic parameters $Y^{\Omega(K,n\Gamma)}_{v\gamma,v'\gamma'}$ of the effective Hamiltonian, Eq. (2) with the specially made computer code SPHETOM. As the result of the analysis, transitions have been assigned for the first time to ten sub-bands of the $3\nu_4$, $\nu_2 + 2\nu_4$ and $2\nu_2 + \nu_4$ bending bands of the tetrad. Unfortunately, in the present study we were not able to assign transitions to the totally forbidden $3\nu_2$ band (all three sub-bands of this band are forbidden by the symmetry of the GeH_4 molecule). The 2955 transitions with the maximum value of upper quantum number $J^{max} = 20$ were assigned to the discussed ten sub-bands of the bending Tetrad of $^{76}GeH_4$ (detailed statistical information about results of assignment can be found in Table 2). The obtained data is a considerable extension of the before known information about spectroscopic properties of the GeH_4 molecule. Complete list of assigned transitions is presented in the Supplementary material. In this case,

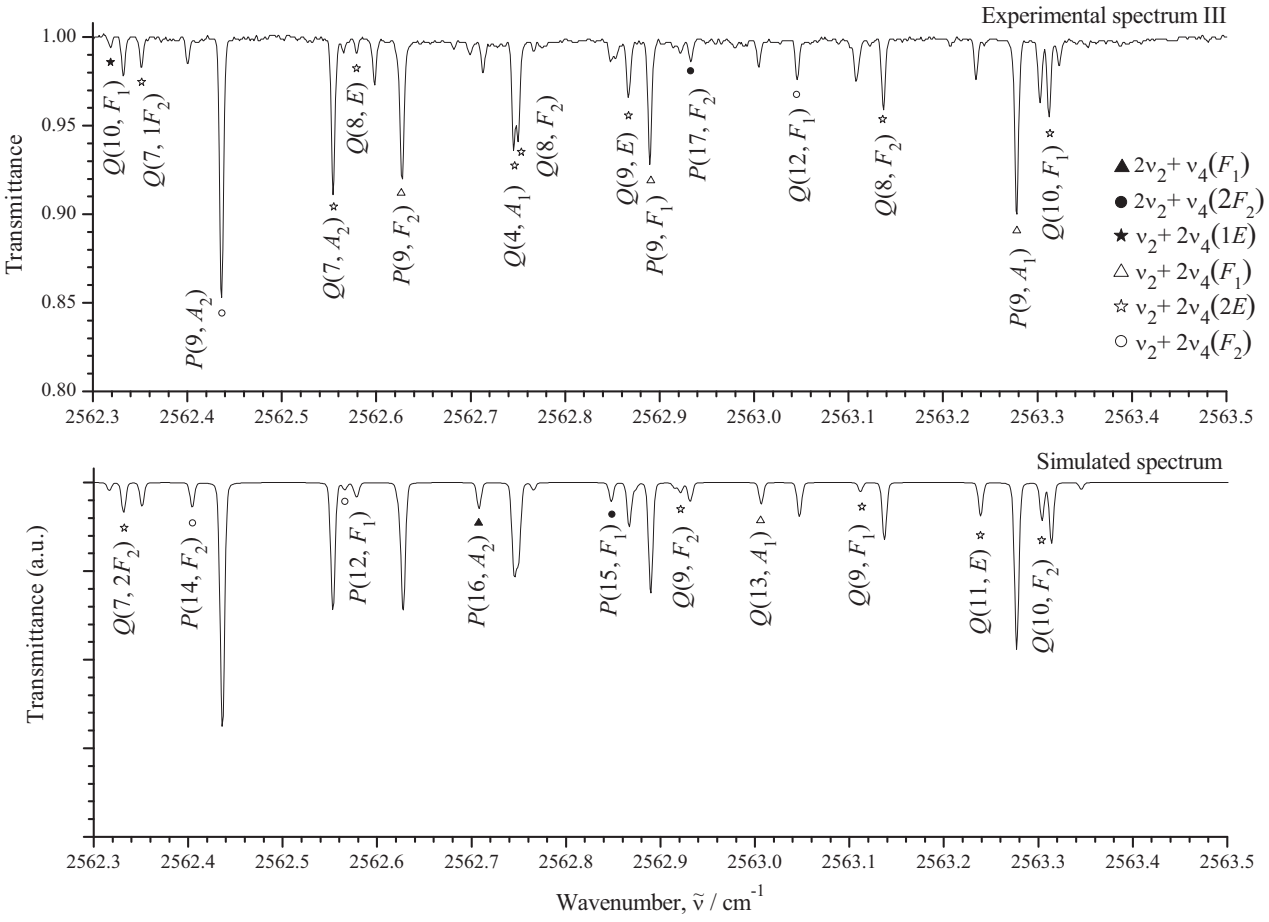

Fig. 5. Small part of the high resolution experimental spectrum III of $^{76}GeH_4$ in the region of the *P* and *Q*-branches of the $\nu_2 + 2\nu_4$ band (top trace). Bottom trace shows the corresponding simulated spectrum. Lines belonging to different sub-bands of the $\nu_2 + 2\nu_4$ band are marked by different symbols (see upper part of the figure for details).

Table 2
Statistical information for the $3\nu_4(1F_2, A_1, F_1, 2F_2)$, $\nu_2 + 2\nu_4(1E, F_1, A_1, F_2, 2E, A_2)$ and $2\nu_2 + \nu_4(1F_2, F_1, 2F_2)$ bands of $^{76}GeH_4$.

Band 1	Energy[a]/cm^{-1} 2	J^{max} 3	N_{tr}[b] 4	N_l[c] 5	m_1[d] 6	m_2[d] 7	m_3[d] 8
$3\nu_4(1F_2)$	2438.2407	20	732	441	64.6	17.7	17.7
$3\nu_4(A_1)$[e]	2456.25						
$3\nu_4(F_1)$	2459.5121	16	147	91	35.4	21.1	43.5
$3\nu_4(2F_2)$	2462.4009	17	242	117	44.6	21.9	33.5
Total N_{tr}			1121				
Total N_l				649			
d_{rms}	7.36×10^{-4} cm^{-1}						
$\nu_2 + 2\nu_4(1E)$	2556.2027	14	223	105	37.7	28.7	33.6
$\nu_2 + 2\nu_4(F_1)$	2567.6835	14	192	104	54.7	21.9	23.4
$\nu_2 + 2\nu_4(A_1)$[e]	2568.97						
$\nu_2 + 2\nu_4(F_2)$	2571.4759	16	137	84	54.0	19.0	27.0
$\nu_2 + 2\nu_4(2E)$	2573.4424	13	43	29	62.8	32.5	4.7
$\nu_2 + 2\nu_4(A_2)$[e]	2576.54						
Total N_{tr}			595				
Total N_l				322			
d_{rms}	6.86×10^{-4} cm^{-1}						
$2\nu_2 + \nu_4(1F_2)$	2675.2299	19	564	329	66.3	20.0	13.7
$2\nu_2 + \nu_4(F_1)$	2681.3912	15	320	167	61.9	25.6	12.5
$2\nu_2 + \nu_4(2F_2)$	2684.1880	16	355	141	56.4	23.9	19.7
Total N_{tr}			1239				
Total N_l				637			
d_{rms}	5.21×10^{-4} cm^{-1}						
$3\nu_2(E)$[e]	2785.41						
$3\nu_2(A_1)$[e]	2791.95						
$3\nu_2(A_2)$[e]	2792.15						

[a] Value of the upper vibrational energy.
[b] N_{tr} is the number of assigned transitions.
[c] N_l is the number of obtained upper-state energies.
[d] Here $m_i = n_i/N_{tr} \times 100\%$ $(i = 1, 2, 3)$; n_1, n_2, and n_3 are the numbers of transitions for which the differences $\delta = \nu^{exp} - \nu^{calc}$ satisfy the conditions $\delta \leq 4 \times 10^{-4}$ cm^{-1}, 4×10^{-4} cm$^{-1} < \delta \leq 7 \times 10^{-4}$ cm^{-1}, and $\delta > 7 \times 10^{-4}$ cm^{-1}.
[e] In the present study transitions have not been assigned to this band. As a consequence, this band was used as a dark one in the fit, and the value of the presented band center was determined from the fit.

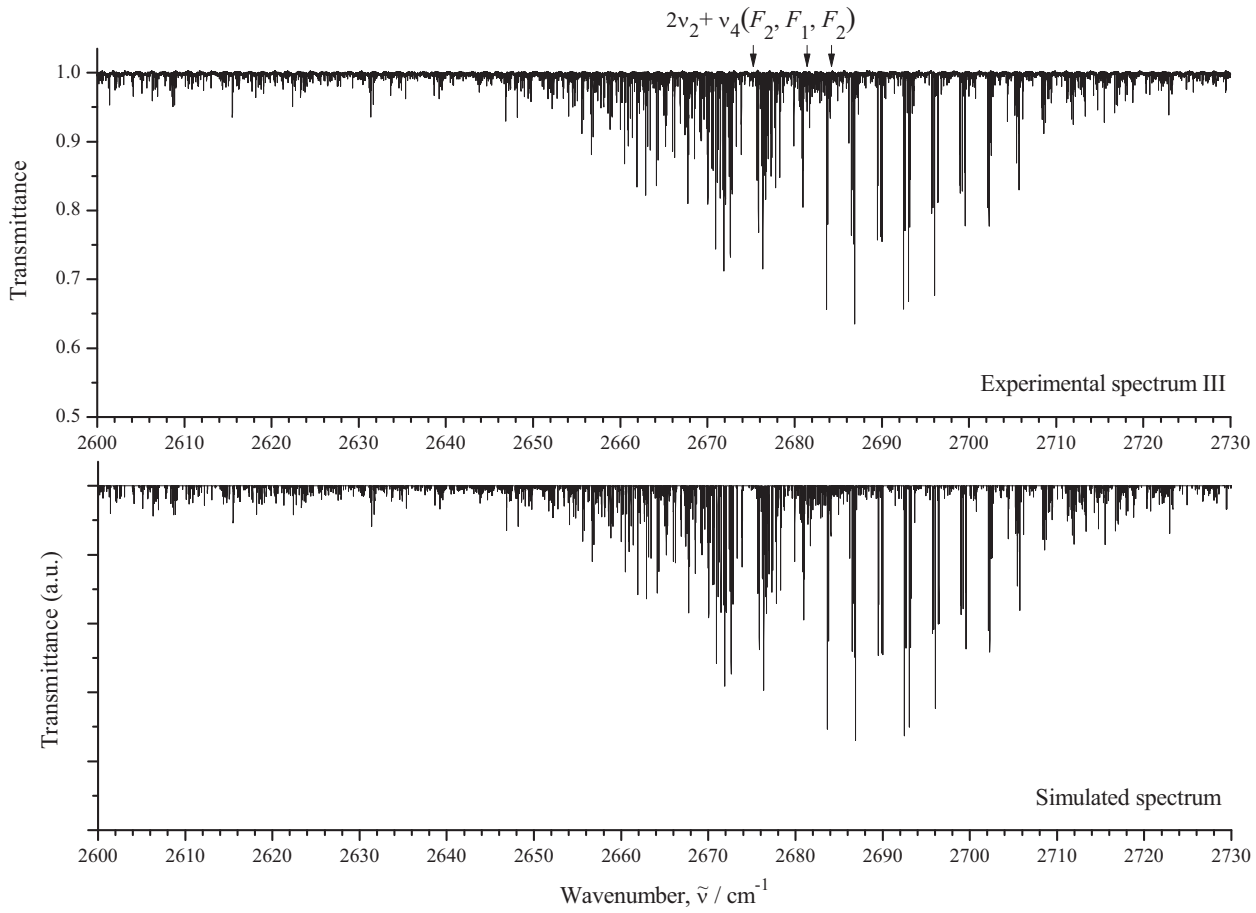

Fig. 6. More in detail overview spectrum III of $^{76}GeH_4$ in the region of the $2\nu_2 + \nu_4$ band (for the experimental conditions, see Section 2). The bottom trace present corresponding simulated spectrum (see text for the conditions of the simulation).

we would like to note that for the convenience of the reader notation of data in the Supplementary material correspond to the XTDS one, Wenger et al. [79] (the XTDS notations have been considered for convenience because the reader is probably less familiar with those of SPHETOM).

5. Ro-vibrational analysis and parameters of the effective Hamiltonian

All the 2955 experimental transitions discussed in the previous section were used as the initial information in the weighted fit procedure to determine the parameters of the effective Hamiltonian given by Eq. (2). As was discussed above, at the first step of the analysis both an assignment and a preliminary fit of spectroscopic parameters were madeusing the SPHETOM code. However the final fit was made on the basis of the XTDS/Dijon software, Wenger et al. [79]. The values of parameters obtained from the fit are presented in column 4 of Table 3 together with their 1σ confidence statistical intervals (the latter are given in parentheses). To give the possibility to use the obtained results by the reader, Tables 4–6 present the values of spectroscopic parameters of the lower ro-vibrational polyads of $^{76}GeH_4$ (the latter are reproduced from [80]; for comparison, columns 5 and 6 of Table 4 present also sets of ground state parameters from Ref. [43] and STDS Dijon package [81,82]). It is necessary to mark that, in spite of the absence of transitions belonging to the $\nu_2 + 2\nu_4(A_1)$, $\nu_2 + 2\nu_4(A_2)$, $3\nu_4(A_1)$, $3\nu_2(A_1)$, $3\nu_2(A_2)$, and $3\nu_2(E)$ sub-bands, all six corresponding vibrational states were taken into account in the fitting procedure as the “dark” ones.

As the result of analysis, 98 spectroscopic parameters from Table 3, obtained from the fit, reproduce 2955 initial experimental line positions of the thirteen ro-vibrational sub-bands of the $^{76}GeH_4$ isotopologue with the $d_{rms} = 6.43 \times 10^{-4}$ cm^{-1}. Corresponding differences are shown in column 5 of the the Supplementary material (see also statistical information in Table 2). Bottom parts of Figs. 1–7 show the simulated spectra which were obtained with the parameters from Table 3. In this case, relative line strengths have been calculated using five effective dipole moment parameters (only one main effective dipole moment parameter for one of five F_2-symmetry band). Relative values of these five main effective dipole moment parameters have been estimated from the specially measured 8–10 line transitions in the experimental spectrum III and, as was found, relate as 6.0:0.9:(−1.1):3.0:1.3 for the bands $(3\nu_4; 1F_2, 2F_2)$, $(\nu_2 + 2\nu_4; F_2)$ and $(2\nu_2 + \nu_4; 1F_2, 2F_2)$. Voigt line shape profile was used in calculations. From a comparison of the top and bottom parts of Figs. 1–7, one can see the good agreement between the experimental and simulated spectra. To give the reader a possibility to appreciate the quality of the results, Fig. 8 shows the fit residuals for line positions as a function of the quantum number J.

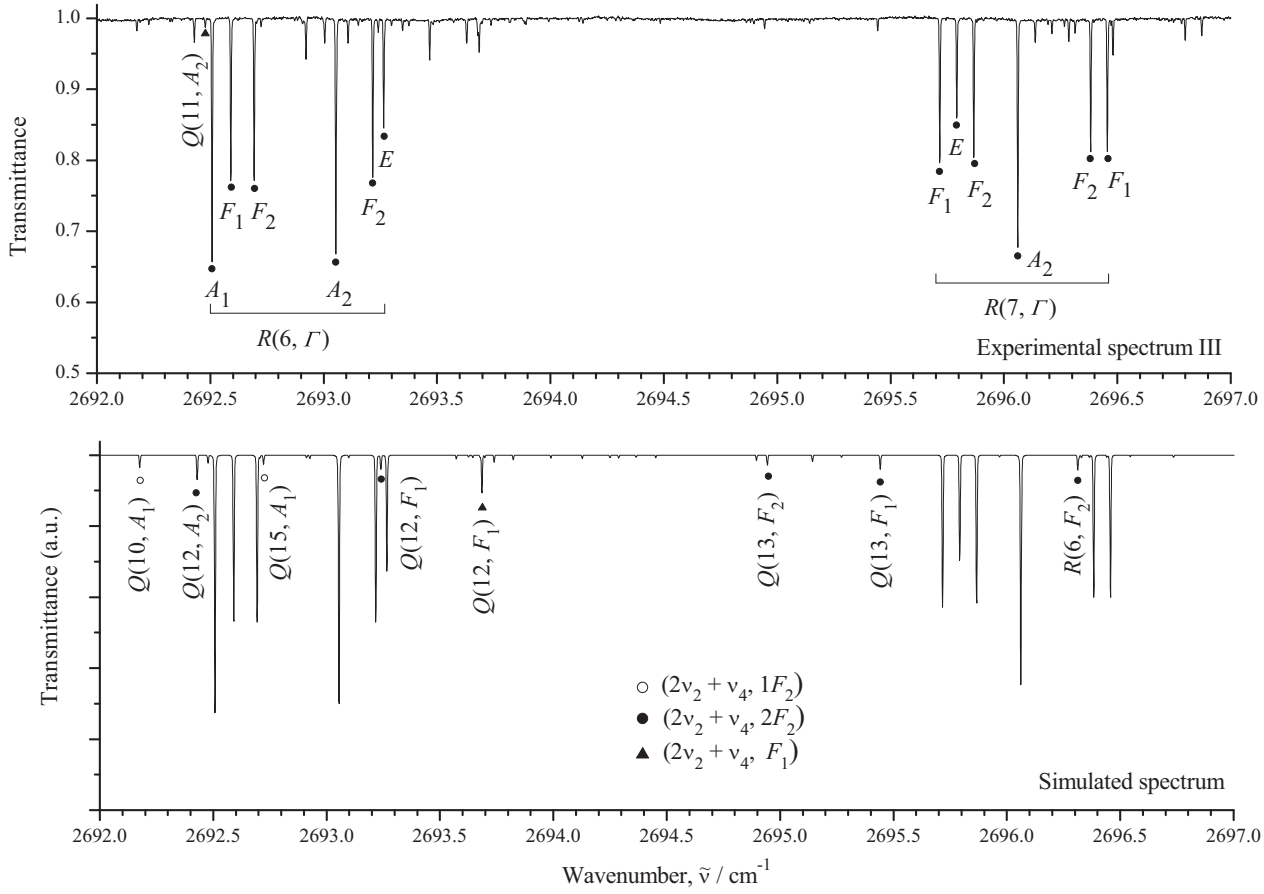

Fig. 7. Small part of the high resolution experimental spectrum III of $^{76}GeH_4$ in the region of the *Q* and *R*-branches of the $2\nu_2 + \nu_4$ band (top trace). Bottom trace shows the corresponding simulated spectrum. Lines belonging to different sub-bands of the $2\nu_2 + \nu_4$ band are marked by different symbols (see lower part of the figure for details).

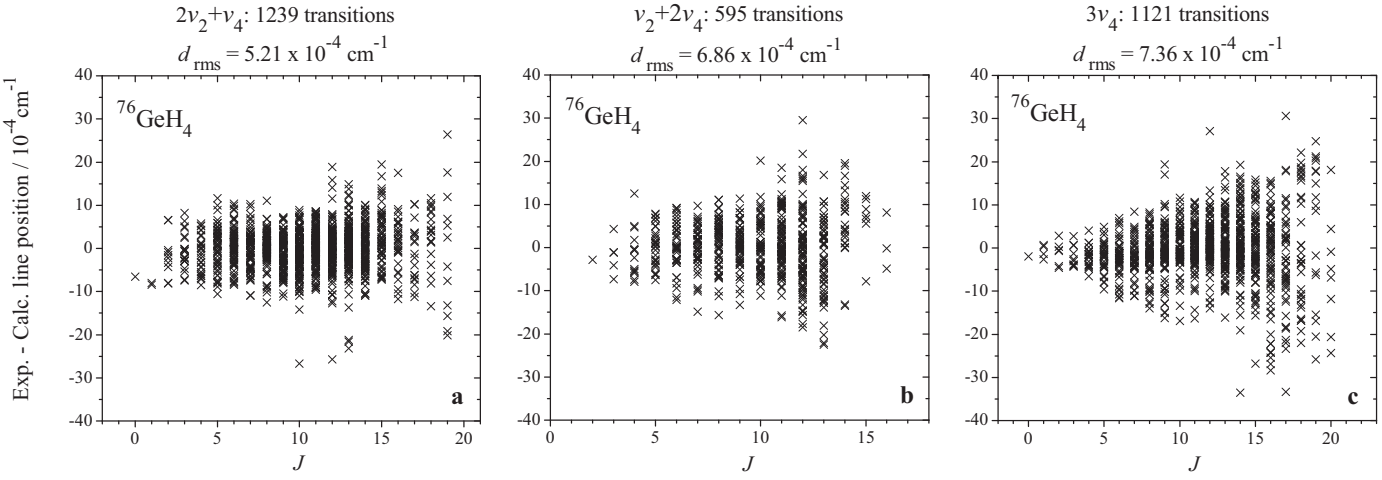

Fig. 8. Observed minus calculated line positions and fit statistics for the bending Tetrad of the ro-vibrational Octad of $^{76}GeH_4$.

Table 3
Spectroscopic parameters $Y^{\Omega(K,n\Gamma)}_{\upsilon\gamma,\upsilon'\gamma'}$ of the (0300)/(0201)/(0102)/(0003) vibrational states of $^{76}GeH_4$ (in cm^{-1})[a].

(υ,γ) 1	(υ',γ') 2	$\Omega(K,n\Gamma)$ 3	$^{76}GeH_4$ 4
(0300,E)	(0300,E)	$0(0,A_1)10^2$	−6.249(16)
(0300,A_1)	(0300,A_1)	$0(0,A_1)10^1$	−3.1675(83)
(0300,A_2)	(0300,A_2)	$0(0,A_1)10^1$	−1.160(12)
(0300,E)	(0201,F_1)	$1(1,F_1)10^3$	−4.700(12)
(0300,A_1)	(0201,F_1)	$1(1,F_1)10^2$	1.0707(21)
(0300,A_2)	(0201,F_2)	$1(1,F_1)10^3$	−6.040(25)
(0201,1F_2)	(0201,1F_2)	$0(0,A_1)10^2$	−6.6284(10)
	(0201,1F_2)	$1(1,F_1)10^3$	1.3965(83)
(0201,1F_2)	(0201,F_1)	$1(1,F_1)10^3$	1.4251(71)
	(0201,F_1)	$2(2,E)10^5$	3.530(18)
(0201,1F_2)	(0201,2F_2)	$0(0,A_1)10^2$	−7.1365(13)
(0201,F_1)	(0201,F_1)	$0(0,A_1)10^2$	−2.5672(18)
	(0201,F_1)	$1(1,F_1)10^3$	2.3085(40)
(0201,F_1)	(0201,1F_2)	$1(1,F_1)10^3$	−5.2568(71)
	(0201,1F_2)	$2(2,E)10^5$	−3.077(30)
(0201,2F_2)	(0201,2F_2)	$0(0,A_1)10^2$	−5.2972(16)
	(0201,2F_2)	$1(1,F_1)10^3$	−1.4003(44)
(0201,1F_2)	(0102,F_1)	$1(1,F_1)10^3$	−5.7282(68)
(0201,1F_2)	(0102,F_2)	$0(0,A_1)10^2$	2.2311(84)
	(0102,F_2)	$1(1,F_1)10^3$	−2.5781(86)
(0201,F_1)	(0102,1E)	$1(1,F_1)10^3$	2.444(10)
(0201,F_1)	(0102,F_1)	$0(0,A_1)10^1$	−1.1439(12)
(0201,F_1)	(0102,F_2)	$1(1,F_1)10^3$	4.306(20)
(0201,2F_2)	(0102,2E)	$1(1,F_1)10^3$	2.144(11)
(0201,2F_2)	(0102,F_1)	$1(1,F_1)10^3$	5.013(20)
(0201,1F_2)	(0003,1F_2)	$1(1,F_1)10^3$	−9.143(38)
(0201,1F_2)	(0003,2F_2)	$0(0,A_1)10^2$	−9.650(11)
(0201,F_1)	(0003,1F_2)	$1(1,F_1)10^2$	1.5223(38)
(0201,F_1)	(0003,A_1)	$1(1,F_1)10^2$	1.3965(37)
(0201,F_1)	(0003,F_1)	$0(0,A_1)10^1$	−2.1123(52)
(0201,F_1)	(0003,2F_2)	$1(1,F_1)10^2$	−2.0540(43)
(0201,2F_2)	(0003,1F_2)	$0(0,A_1)10^1$	−2.2070(22)
(0201,2F_2)	(0003,A_1)	$2(2,F_2)10^4$	−2.424(15)
(0201,2F_2)	(0003,F_1)	$1(1,F_1)10^2$	−1.5157(43)
(0102,1E)	(0102,1E)	$0(0,A_1)10^1$	−2.02116(25)
	(0102,1E)	$2(0,A_1)10^5$	4.918(28)
(0102,1E)	(0102,A_2)	$2(2,E)10^5$	−9.731(40)
(0102,1E)	(0102,2E)	$0(0,A_1)10^2$	1.7965(44)
	(0102,2E)	$2(0,A_1)10^5$	−2.971(35)
(0102,1E)	(0102,F_1)	$1(1,F_1)10^3$	7.011(14)
(0102,1E)	(0102,F_2)	$1(1,F_1)10^3$	−9.569(15)
	(0102,F_2)	$2(2,F_2)10^5$	4.798(37)
(0102,A_1)	(0102,A_1)	$0(0,A_1)10^2$	−5.3854(48)
(0102,A_1)	(0102,F_1)	$1(1,F_1)10^2$	1.0346(11)
(0102,A_2)	(0102,A_2)	$0(0,A_1)10^2$	−4.6393(43)
(0102,A_2)	(0102,2E)	$2(2,E)10^5$	−5.693(33)
(0102,A_2)	(0102,F_2)	$1(1,F_1)10^3$	−2.7899(84)
(0102,2E)	(0102,2E)	$0(0,A_1)10^2$	1.6151(43)
(0102,2E)	(0102,F_1)	$1(1,F_1)10^3$	−1.973(11)
	(0102,F_1)	$2(2,F_2)10^5$	7.552(49)
(0102,2E)	(0102,F_2)	$1(1,F_1)10^4$	2.355(73)
(0102,F_1)	(0102,F_1)	$0(0,A_1)10^1$	−1.30480(57)
	(0102,F_1)	$1(1,F_1)10^3$	7.640(20)
	(0102,F_1)	$2(0,A_1)10^5$	2.925(50)
(0102,F_1)	(0102,F_2)	$1(1,F_1)10^2$	−1.4052(18)
	(0102,F_2)	$2(2,E)10^5$	−6.705(37)
(0102,F_2)	(0102,F_2)	$0(0,A_1)10^2$	−3.7187(35)
	(0102,F_2)	$2(0,A_1)10^5$	−1.597(41)
(0102,1E)	(0003,1F_2)	$2(2,F_2)10^5$	4.619(43)
(0102,1E)	(0003,2F_2)	$1(1,F_1)10^3$	−8.104(17)
(0102,A_1)	(0003,F_1)	$1(1,F_1)10^3$	−6.853(32)
(0102,A_1)	(0003,2F_2)	$2(2,F_2)10^4$	2.6442(90)
(0102,A_2)	(0003,1F_2)	$1(1,F_1)10^2$	1.4413(24)
(0102,A_2)	(0003,F_1)	$2(2,F_2)10^5$	−5.936(82)
(0102,2E)	(0003,1F_2)	$1(1,F_1)10^3$	8.499(22)
(0102,2E)	(0003,2F_2)	$1(1,F_1)10^3$	−2.315(12)
(0102,F_1)	(0003,A_1)	$1(1,F_1)10^3$	−9.029(28)
(0102,F_1)	(0003,F_1)	$0(0,A_1)10^1$	1.5196(32)
	(0003,F_1)	$1(1,F_1)10^3$	1.817(16)
(0102,F_1)	(0003,2F_2)	$1(1,F_1)10^2$	1.8650(39)
	(0003,2F_2)	$2(2,E)10^5$	6.32(11)
(0102,F_2)	(0003,1F_2)	$0(0,A_1)10^1$	−1.9871(22)
	(0003,1F_2)	$1(1,F_1)10^3$	7.920(22)
	(0003,1F_2)	$2(0,A_1)10^5$	−6.979(40)
(0102,F_2)	(0003,F_1)	$1(1,F_1)10^2$	−1.7755(28)
	(0003,F_1)	$2(2,E)10^4$	−1.1936(74)

Table 3 (*continued*)

(υ,γ) 1	(υ',γ') 2	$\Omega(K,n\Gamma)$ 3	$^{76}GeH_4$ 4
(0102,F_2)	(0003,2F_2)	$0(0,A_1)10^2$	8.593(10)
	(0003,2F_2)	$1(1,F_1)10^3$	3.880(12)
(0102,F_2)	(0003,2F_2)	$2(0,A_1)10^4$	−1.1744(62)
(0003,1F_2)	(0003,1F_2)	$0(0,A_1)10^1$	−2.367679(99)
	(0003,1F_2)	$1(1,F_1)10^3$	7.0419(99)
	(0003,1F_2)	$2(0,A_1)10^5$	−2.704(21)
	(0003,1F_2)	$2(2,E)10^4$	−1.0838(27)
	(0003,1F_2)	$2(2,F_2)10^5$	5.433(41)
(0003,1F_2)	(0003,A_1)	$2(2,F_2)10^4$	−1.6609(57)
(0003,1F_2)	(0003,F_1)	$1(1,F_1)10^3$	9.689(14)
	(0003,F_1)	$2(2,E)10^4$	−1.9745(49)
(0003,1F_2)	(0003,2F_2)	$0(0,A_1)10^2$	−8.8403(24)
	(0003,2F_2)	$2(0,A_1)10^4$	−2.2784(48)
	(0003,2F_2)	$2(2,E)10^4$	−3.7255(62)
(0003,A_1)	(0003,A_1)	$0(0,A_1)10^2$	−5.1090(61)
(0003,A_1)	(0003,F_1)	$1(1,F_1)10^3$	−9.378(14)
(0003,F_1)	(0003,F_1)	$0(0,A_1)10^2$	3.3177(57)
	(0003,F_1)	$1(1,F_1)10^2$	−1.0649(22)
	(0003,F_1)	$2(0,A_1)10^5$	−5.435(48)
(0003,F_1)	(0003,2F_2)	$1(1,F_1)10^3$	−1.3668(87)
(0003,2F_2)	(0003,2F_2)	$0(0,A_1)10^2$	−2.6773(30)
	(0003,2F_2)	$2(0,A_1)10^5$	5.216(35)

[a] Values in parenthesis are 1σ statistical standard errors.

Table 4
Spectroscopic parameters $Y^{\Omega(K,n\Gamma)}_{\upsilon\gamma,\upsilon'\gamma'}$ of the ground state of $^{76}GeH_4$ (in cm^{-1}).

(υ,γ) 1	(υ',γ') 2	$\Omega(K,n\Gamma)$ 3	$^{76}GeH_4$[a] 4	GeH_4[b] 5	GeH_4[c] 6
$(0000,A_1)$	$(0000,A_1)$	$2(0,A_1)$	2.695870305	2.6958644	2.695861
$(0000,A_1)$	$(0000,A_1)$	$4(0,A_1)10^4$	−0.3341682	−0.33418	−0.3336
$(0000,A_1)$	$(0000,A_1)$	$4(4,A_1)10^5$	−0.1547079	−0.15464	−0.154785
$(0000,A_1)$	$(0000,A_1)$	$6(0,A_1)10^8$	0.114368	0.1142	0.106
$(0000,A_1)$	$(0000,A_1)$	$6(4,A_1)10^{10}$	−0.51075	−0.497	−0.5325649
$(0000,A_1)$	$(0000,A_1)$	$6(6,A_1)10^{10}$	−0.15638	−0.1600	−0.1666028
$(0000,A_1)$	$(0000,A_1)$	$8(4,A_1)10^{14}$			−0.17261
$(0000,A_1)$	$(0000,A_1)$	$8(6,A_1)10^{14}$			−0.10296
$(0000,A_1)$	$(0000,A_1)$	$8(8,A_1)10^{15}$			−0.14375

[a] Reproduced from Ref. [80].
[b] Reproduced from Ref. [43].
[c] Reproduced from Refs. [81,82].

Table 5
Spectroscopic parameters $Y^{\Omega(K,n\Gamma)}_{\upsilon\gamma,\upsilon'\gamma'}$ of the (0100)/(0001) vibrational states of $^{76}GeH_4$ (in cm^{-1})[a].

(υ,γ) 1	(υ',γ') 2	$\Omega(K,n\Gamma)$ 3	$^{76}GeH_4$ 4
$(0100,E)$	$(0100,E)$	$0(0,A_1)$	929.9130275
	$(0100,E)$	$2(2,E)10^1$	−0.1078743
	$(0100,E)$	$3(3,A_2)10^4$	0.22618
	$(0100,E)$	$4(0,A_1)10^6$	−0.4052
	$(0100,E)$	$4(2,E)10^6$	−0.31077
	$(0100,E)$	$4(4,A_1)10^7$	0.134
	$(0100,E)$	$4(4,E)10^6$	−0.12583
$(0100,E)$	$(0001,F_2)$	$1(1,F_1)$	−4.503062
	$(0001,F_2)$	$2(2,F_2)$	−0.0213168
	$(0001,F_2)$	$3(1,F_1)10^3$	−0.1179267
	$(0001,F_2)$	$3(3,F_2)10^4$	0.138096
	$(0001,F_2)$	$4(2,F_2)10^6$	−0.2122
	$(0001,F_2)$	$4(4,F_1)10^6$	−0.18552
	$(0001,F_2)$	$4(4,F_2)10^6$	−0.209879
	$(0001,F_2)$	$5(1,F_1)10^8$	−0.23013
	$(0001,F_2)$	$5(3,F_1)10^8$	0.13677
	$(0001,F_2)$	$5(3,F_2)10^9$	0.5885
$(0001,F_2)$	$(0001,F_2)$	$0(0,A_1)$	820.3270025
	$(0001,F_2)$	$1(1,F_1)$	6.39186203
	$(0001,F_2)$	$2(0,A_1)10^2$	0.1060455
	$(0001,F_2)$	$2(2,E)10^2$	−0.14849411
	$(0001,F_2)$	$2(2,F_2)$	−0.0106923
	$(0001,F_2)$	$3(1,F_1)10^4$	0.70545
	$(0001,F_2)$	$3(3,F_1)10^4$	−0.47902
	$(0001,F_2)$	$4(0,A_1)10^6$	−0.3653
	$(0001,F_2)$	$4(2,F_2)10^6$	−0.3519
	$(0001,F_2)$	$4(4,A_1)10^7$	−0.6407
	$(0001,F_2)$	$5(1,F_1)10^8$	0.25953
	$(0001,F_2)$	$5(3,F_1)10^8$	−0.16967
	$(0001,F_2)$	$6(0,A_1)10^{10}$	0.4276

[a] Reproduced from Ref. [80].

Table 6
Spectroscopic parameters $Y^{\Omega(K,n\Gamma)}_{v\gamma,v'\gamma'}$ of the set of interacting vibrational states (0002)(0101)/(0200) in $^{76}GeH_4$ (in cm^{-1})[a].

(v,γ) 1	(v',γ') 2	$\Omega(K,n\Gamma)$ 3	$^{76}GeH_4$ 4
$(0200,A_1)$	$(0200,A_1)$	$0(0,A_1)$	−2.68369
	$(0200,A_1)$	$2(0,A_1)10^3$	−0.4716
$(0200,A_1)$	$(0200,E)$	$2(2,E)10^3$	−0.255550
$(0200,E)$	$(0200,E)$	$0(0,A_1)$	0.8410781
	$(0200,E)$	$2(2,E)10^3$	0.3393
	$(0200,E)$	$3(3,A_2)10^5$	0.26045
$(0200,A_1)$	$(0101,F_2)$	$2(2,F_2)10^3$	−0.118
$(0200,E)$	$(0101,F_1)$	$1(1,F_1)$	0.0268263
	$(0101,F_1)$	$2(2,F_2)10^3$	−0.21017
	$(0101,F_1)$	$3(3,F_2)10^5$	−0.4234
$(0200,E)$	$(0101,F_2)$	$1(1,F_1)$	0.0319736
	$(0101,F_2)$	$3(1,F_1)10^5$	−0.4543
$(0200,A_1)$	$(0002,A_1)$	$0(0,A_1)$	−5.45261
	$(0002,A_1)$	$2(0,A_1)10^3$	0.54198
$(0200,E)$	$(0002,E)$	$0(0,A_1)$	0.15817
	$(0002,E)$	$2(2,E)10^3$	0.47525
$(0200,E)$	$(0002,F_2)$	$1(1,F_1)$	0.2314435
	$(0002,F_2)$	$3(1,F_1)10^5$	−0.3016
$(0101,F_1)$	$(0101,F_1)$	$0(0,A_1)$	2.2635159
	$(0101,F_1)$	$1(1,F_1)$	−0.0510521
	$(0101,F_1)$	$2(0,A_1)10^5$	−0.509
	$(0101,F_1)$	$2(2,F_2)10^3$	−0.7694
$(0101,F_1)$	$(0101,F_2)$	$1(1,F_1)$	−0.0562747
	$(0101,F_2)$	$2(2,E)10^4$	0.7774
	$(0101,F_2)$	$2(2,F_2)10^3$	0.79071
	$(0101,F_2)$	$3(1,F_1)10^5$	−0.58181
$(0101,F_2)$	$(0101,F_2)$	$0(0,A_1)$	−2.013554
	$(0101,F_2)$	$1(1,F_1)$	−0.0546425
	$(0101,F_2)$	$2(0,A_1)10^3$	−0.378256
	$(0101,F_2)$	$2(2,E)10^3$	0.3357
	$(0101,F_2)$	$2(2,F_2)10^3$	−0.8515
	$(0101,F_2)$	$3(1,F_1)10^4$	−0.18456
	$(0101,F_2)$	$3(3,F_1)10^4$	−0.14931
$(0101,F_1)$	$(0002,A_1)$	$1(1,F_1)$	0.0659491
$(0101,F_1)$	$(0002,E)$	$1(1,F_1)10^3$	0.2899
$(0101,F_1)$	$(0002,F_2)$	$1(1,F_1)10^2$	−0.08504
	$(0002,F_2)$	$2(2,E)10^3$	0.15676
	$(0002,F_2)$	$2(2,F_2)10^5$	0.1592
	$(0002,F_2)$	$3(1,F_2)10^5$	−0.2948
	$(0002,F_2)$	$3(3,A_2)10^5$	0.3359
	$(0002,F_2)$	$3(3,F_1)10^5$	−0.9951
	$(0002,F_2)$	$3(3,F_2)10^6$	0.692
$(0101,F_2)$	$(0002,A_1)$	$2(2,F_2)10^3$	0.3879
	$(0002,A_1)$	$3(3,F_2)10^5$	−0.2470
$(0101,F_2)$	$(0002,E)$	$3(1,F_1)10^4$	−0.14208
$(0101,F_2)$	$(0002,F_2)$	$0(0,A_1)$	−4.299716
	$(0002,F_2)$	$1(1,F_1)$	0.0258758
	$(0002,F_2)$	$2(0,A_1)10^3$	0.63352
	$(0002,F_2)$	$2(2,E)10^4$	−0.2856
	$(0002,F_2)$	$3(1,F_1)10^5$	−0.13014
	$(0002,F_2)$	$3(3,F_2)10^4$	0.14725
$(0002,A_1)$	$(0002,A_1)$	$0(0,A_1)$	−13.029825
	$(0002,A_1)$	$2(0,A_1)10^4$	0.1675
$(0002,A_1)$	$(0002,E)$	$2(2,E)10^3$	0.22230
$(0002,A_1)$	$(0002,F_2)$	$2(2,F_2)10^3$	−0.30745
	$(0002,F_2)$	$3(3,F_2)10^4$	0.10809
$(0002,E)$	$(0002,E)$	$0(0,A_1)$	1.488355
	$(0002,E)$	$2(2,E)10^3$	−0.52025
	$(0002,E)$	$3(3,A_2)10^4$	0.10591
$(0002,E)$	$(0002,F_2)$	$1(1,F_1)$	0.0301450
	$(0002,F_2)$	$2(2,F_2)10^3$	−0.60036
	$(0002,F_2)$	$3(1,F_1)10^6$	−0.353
	$(0002,F_2)$	$3(3,F_1)10^5$	−0.196
	$(0002,F_2)$	$3(3,F_2)10^5$	−0.5111
$(0002,F_2)$	$(0002,F_2)$	$0(0,A_1)$	−1.227372
	$(0002,F_2)$	$1(1,F_1)$	−0.0330432
	$(0002,F_2)$	$2(0,A_1)10^4$	−0.1478
	$(0002,F_2)$	$2(2,E)10^3$	0.119
	$(0002,F_2)$	$2(2,F_2)10^3$	0.58023
	$(0002,F_2)$	$3(1,F_1)10^6$	−0.3567
	$(0002,F_2)$	$3(3,F_1)10^5$	−0.5775

[a] Reproduced from Ref. [80].

6. Conclusion

High resolution FTIR spectra of the $^{76}GeH_4$ molecules enriched up to 88.1% were recorded with a Bruker IFS 125HR Fourier transform spectrometer in the region of bending tetrad of the octad. Ro-vibrational transitions belonging to the ten sub-bands of the three bending bands, $3\nu_4$, $\nu_2+2\nu_4$ and $2\nu_2+\nu_4$, of the tetrad were assigned in the experimental spectra. On that basis, 2955 transitions with the maximum value of upper quantum number $J^{max}=20$ were assigned to these thirteen sub-bands. The obtained data were used in a weighted fitting procedure to determine the spectroscopic parameters of the effective Hamiltonian. A set of 98 spectroscopic parameters obtained from the fit reproduced 2955 initial experimental line positions with a $d_{rms}=6.43\times10^{-4}\,cm^{-1}$.

Declaration of Competing Interest

Authors declare that they have no conflict of interest.

CRediT authorship contribution statement

O.N. Ulenikov: Conceptualization, Supervision, Writing - review & editing, Methodology, Investigation, Writing - original draft. **O.V. Gromova:** Methodology, Software, Investigation. **E.S. Bekhtereva:** Methodology, Software, Investigation. **N.I. Raspopova:** Validation, Investigation. **I.A. Velmuzhova:** Validation, Investigation, Resources. **M.A. Koshelev:** Validation, Investigation, Resources. **P.G. Sennikov:** Validation, Investigation, Resources.

Acknowledgments

Study was funded by the Tomsk Polytechnic University Competitiveness Enhancement Program (project VIU189/2020).

Supplementary material

Supplementary material associated with this article can be found, in the online version, at doi:10.1016/j.jqsrt.2021.107517.

References

[1] Asplund M, Grevesse N, Sauval J, Scott P. The chemical composition of the sun. Ann Rev Astron Astrophys 2009;47:451–522.
[2] Corice RJ, Fox JR, Fox K. The hypothetical chemical and spectroscopic activity of germane in the atmosphere of Jupiter. Icarus 1972;16:388–91.
[3] Fink U, Larson HP, Treffers RR. Germane in the atmosphere of Jupiter. Icarus 1978;34:344–54.
[4] Kunde V, Hanel R, Maguire W, Gautier D, Baluteau J-P, Marten A, Chédin A, Husson N, Scott N. The tropospheric gas composition of the North Equatorial Belt (NH_3, PH_3, CH_3D, GeH_4, H_2O) and the Jovian D/H isotopic ratio. Astrophys J 1982;263:443–67.
[5] Drossart P, Encrenaz T, Kunde V, Hanel R, Combes M. An estimate of the PH_3, NH_3, CH_3d and GeH_4 abundances on Jupiter from the Voyager IRIS data at 4.5 μm. Icarus 1982;49:416–26.
[6] Chen F, Judge DL, Wu CYR, Caldwell J, White HP, Wagener R. High-resolution, low–temperature photoabsorption cross sections of C_2H_2, PH_3, AsH_3, and GeH_4 with application to Saturn's atmosphere. J Geophys Res 1991;96:17519–27.
[7] Atreya SK, Mahaffy PR, Niemann HB, Wong MH, Owen TC. Composition and origin of the atmosphere of Jupiter– an update, and implications for the extra-solar giant planets. Planet Space Sci 2003;51:105–12.
[8] Lodders K. Jupiter formed with more tar than ice. Astrophys J 2004;611:587–97.
[9] Lodders K. Atmospheric chemistry of the gas giant planets. Geochem Soc 2010. http://www.geochemsoc.org/publications/geochemicalnews/gn142jan10/atmosphericchemistryoftheg/.
[10] Haller EE. Germanium: From its discovery to SiGe devices. Mater Sci Semicond Process 2006;9:408–22.
[11] Agostini M, Allardt M, Andreotti E, Bakalyarov AM, Balata M, Barabanov I, et al. The background in the $0\nu\beta\beta$ experiment GERDA. Eur Phys J 2014;74:1–25.

[12] Quack M. Concept of law in chemistry: the concept of law and models in chemistry. Eur Rev 2014;22:S50–86.
[13] Schwarz H. Chemistry with methane: concepts rather than recipes. Angew Chem 2011;50:10096–115.
[14] Thyagarajan G, Herranz J, Cleveland FF. Potenial energy constants and rotational distortion constants for SiH_4, SiD_4, GeH_4, and GeD_4. J Mol Spectrosc 1961;7:154–8.
[15] Bekhtereva E.S., Gromova O.V., Fomchenko A.L., Bauerecker S.. Precise semi–empirical intramolecular potential surface of GeH_4. Phys Chem Chem Phys(in preparation 2021).
[16] Nikitin AV, Rey M, Rodina A, Krishna BM, Tyuterev VG. Full–dimensional potential energy and dipole moment surfaces of GeH_4 molecule and accurate first–principle rotationally resolved intensity predictions in the infrared. J Phys Chem A 2016;45:8983–97.
[17] Corice RJ Jr., Fox K, Fletcher WH. Studies of absorption spectra of GeH_4 in the 2–17 μ region. J Mol Struct 1972;41:95–104.
[18] Kattenberg HW, Gabes W, Oskam A. Infrared and laser raman gas spectra of GeH_4. J Mol Spectrosc 1972;44:425–42.
[19] Ozier IO, Rosenberg A. The forbidden rotational spectrum of GeH_4 in the ground vibronic state. Can J Phys 1973;51(17):1882–95.
[20] Lepage P, Brégier R, Saint-Loup R. La bande ν_3 du germane. C R Acad Sci Ser B 1976;283:179–80.
[21] Kreiner WA, Andresen U, Oka T. Infrared–microwave double resonance spectroscopy of GeH_4. J Chem Phys 1977;66:4662–5.
[22] Kreiner WA, Orr BJ, Andresen U, Oka T. Measurement of the centrifugal–distortion dipole moment of GeH_4 using a CO_2 laser. Phys Rev A 1977;15:2298–304.
[23] Daunt SJ, Halsey GW, Fox K, Lovell RJ, Gailar NM. High–resolution infrared spectra of ν_3 and $2\nu_3$ of germane. J Chem Phys 1978;68:1319–21.
[24] Corice RJ. Theoretical absolute J-manifold intensities of the ν_3 fundamental of GeH_4. J Quant Spectrosc Radiat Transf 1978;20:65–9.
[25] Kagann RH, Ozier I, McRae GA, Gerry MCL. The distortion moment spectrum of GeH_4: the microwave q branch. Can J Phys 1979;57:593–600.
[26] Fox K, Halsey GW, Daunt SJ, Kennedy RC. Transition moment for ν_3 of $^{74}GeH_4$. J Chem Phys 1979;70:5326–7.
[27] Kreiner WA, Magerl G, Furch B, Bonek E. IR laser sideband observations in GeH_4 and CD_4. J Chem Phys 1979;70:5016–20.
[28] Magerl G, Schupita W, Bonek E, Kreiner WA. Observation of the isotope effect in the ν_2 fundamental of germane. J Chem Phys 1980;72:395–8.
[29] Kreiner WA, Opferkuch R, Robiette AG, Turner PH. The ground-state rotational constants of germane. J Mol Spectrosc 1981;85:442–8.
[30] Lepage P, Champion JP, Robiette AG. Analysis of the ν_3 and ν_1 infrared bands of GeH_4. J Mol Spectrosc 1981;89:440–8.
[31] Das PP, Malathy Devi V, Narahari Rao K, Robiette AG. Tunable diode laser study of the ν_4 infrared band of GeH_4. J Mol Spectrosc 1982;91:494–8.
[32] Schaeffer RD, Lovejoy RW. Absolute line strengths of $^{74}GeH_4$ near 5 μm. J Mol Spectrosc 1985;113:310–14.
[33] Cadot J. Line strengths and pressure broadening by hydrogen in the spectrum of germane near 2110 cm^{-1}. J Quant Spectrosc Radiat Transf 1985;34:331–4.
[34] Varanasi P, Chudamani S. Intensities and H_2-broadened half–widths of germane lines around 4.7 μm at temperatures relevant to Jupiter's atmosphere. J Quant Spectrosc Radiat Transf 1987;38:173–7.
[35] Zhu Q, Thrush BA, Robiette AG. Local mode rotational structure in the (3000) Ge–H stretching overtone ("$3\nu_3$") of germane. Chem Phys Lett 1988;150:181–3.
[36] Halonen L. Stretching vibrational states in germane. J Phys Chem 1989;93:631–4.
[37] Zhu Q, Thrush BA. Rotational structure near the local mode limit in the (3000) band of germane. J Chem Phys 1990;92:2691–7.
[38] Zhu Q, Qian H, Thrush BA. Rotational analysis of the (2000) and (3000) bands and vibration-rotation interaction in germane local mode states. Chem Phys Lett 1991;186:436–40.
[39] Campargue A, Vetterhöffer J, Chenevier M. Rotationally resolved overtone transitions of $^{70}GeH_4$ in the visible and near-infrared. Chem Phys Lett 1992;192:353–6.
[40] Zhu Q, Campargue A, Vetterhöffer J, Permogorov D, Stoeckel F. High resolution spectra of $GeH_4 \nu = 6$ and 7 stretch overtones. the perturbed local mode vibrational states. J Chem Phys 1993;99:2359–64.
[41] Sun F, Wang X, Liao J, Zhu Q. The (5000) local mode vibrational state of germane: ahigh-resolution spectroscopic study. J Mol Spectrosc 1997;184:12–21.
[42] Chen XY, Lin H, Wang XG, Deng K, Zhu QS. High–resolution fourier transform spectrum of the (4000) local mode overtone of GeH_4: local mode effect. J Mol Struct 2000;517–518:41–51.
[43] Boudon V, Grigoryan T, Philipot F, Richard C, Kwabia Tchana F, Manceron L, et al. Line positions and intensities for the ν_3 band of 5 isotopologues of germane for planetary applications. J Quant Spectrosc Radiat Transf 2018;205:174–83.
[44] Richard C, Boudon V, Rotger M. Calculated spectroscopic databases for the VAMDC portal: new molecules and improvements. J Quant Spectrosc Radiat Transfer 2020;251:107096.
[45] Champion J-P, Hilico J-C, Wenger C. Analysis of the ν_2/ν_4 dyad of $^{12}CH_4$ and $^{13}CH_4$. J Mol Spectrosc 1989;133:256–72.
[46] Hilico J-C, Robert O, Loëte M, Toumi S, Pine AS, Brown LR. Analysis of the interacting octad system of $^{12}CH_4$. J Mol Spectrosc 2001;208:1–13.
[47] Ulenikov ON, Ushakova GA. Analysis of the H_2O molecule second–hexade interacting vibrational states. J Mol Spectrosc 1986;117:195–205.
[48] Ulenikov ON, Malikova AB, Li H-F, Qian H-B, Zhu QS, Thrush B. High–resolution spectroscopic study of $2\nu_1$, $2\nu_3$, and $\nu_1 + \nu_3$ stretching states: the local–mode effects of H_2Se. J Chem Soc Faraday Trans 1995;91:13–16.
[49] Wang X-H, Ulenikov ON, Onopenko GA, Bekhtereva ES, He S-G, Hu S-M, Lin H, Zhu Q-S. High–resolution study of the first hexad of D_2O. J Mol Spectrosc 2000;200:25–33.
[50] Ulenikov ON, Gromova OV, Bekhtereva ES, Maul C, Bauerecker S, Gabona MG, Tan TL. High resolution ro–vibrational analysis of interacting bands ν_4, ν_7, ν_{10}, and ν_{12} of $^{13}C_2H_4$. J Mol Spectrosc 2015;151:224–38.
[51] Ulenikov ON, Bekhtereva ES, Gromova OV, Buttersack T, Sydow C, Bauerecker S. High resolution FTIR study of $^{34}S^{16}O_2$: the bands $2\nu_1$, $\nu_1 + \nu_3$, $\nu_1 + \nu_2 + \nu_3 - \nu_2\nu_1 + \nu_2 + \nu_3$. J Quant Spectrosc Radiat Transfer 2016;169:49–57.
[52] Bolotova IB, Ulenikov ON, Bekhtereva ES, Albert S, Chen Z, Hollenstein H, Zindel D, Quack M. High resolution fourier transform infrared spectroscopy of the ground state, ν_3, $2\nu_3$, ν_4 levels of $^{13}CHF_3$. J Mol Spectrosc 2017;337:96–104.
[53] Gordon IE, Rothman LS, Hill C, Kochanov RV, Tan Y, Bernath PF, et al. The HITRAN 2016 molecular spectroscopic database. J Quant Spectrosc Radtat Transf 2017;203:3–69.
[54] Hecht T. The vibration-rotation energies of tetrahedral XY_4 molecules. Part I. Theory of spherical top molecules. J Mol Spectrosc 1960;5:355–89.
[55] Niederer HM. The infrared spectrum of methane. München: Verlag Dr Hut; 2012.
[56] Niederer HM, Wang XG, Carrington T, Albert S, Bauerecker S, Boudon V, Quack M. Analysis of the rovibrational spectrum of $^{13}CH_4$ in the octad range. J Mol Spectrosc 2013;291:33–47.
[57] Fano U, Racah G. Irreducible tensorial sets. New York: Academic Press; 1959.
[58] Wigner EP. Quantum theory of angular momentum. New York: Academic Press; 1965.
[59] Varshalovitch DA, Moskalev AN, Khersonsky VK. Quantum theory of angular momentum. Leningrad: Nauka; 1975.
[60] Silver B. Irreducible tensorial methods. New York–London: Academic Press; 1976.
[61] Boudon V, Champion JP, Gabard T, Loëte M, Rotger M, Wenger C. Spherical top theory and molecular spectra. In: Quack M, Merkt F, editors. Handbook of high–resolution spectroscopy, 3. Wiley; 2011. p. 1437–60.
[62] Moret-Bailly J. Sur l'interprétation des spectres de vibration-rotation des molécules à symmétrie tétraédrique ou octaédrique. Cah Phys 1961;15:238–314.
[63] Champion JP, Pierre G, Michelot F, Moret-Bailly J. Composantes cubiques normales des tenseurs spheriques. Can J Phys 1977;55:512–20.
[64] Champion JP. Developpement complet de l'hamiltonien de vibration-rotation adapté à 1'étude des interactions dans les molécules toupies sphériques. application aux bandes ν_2 et ν_4 de $^{12}CH_4$. Can J Phys 1977;55:1802–28.
[65] Boudon V, Champion JP, Gabard T, Loëte M, Michelot F, Pierre G, Rotger M, Wenger C, Rey M. Symmetry–adapted tensorial formalism to model rovibrational and rovibronic spectra of molecules pertaining to various point groups. J Mol Spectrosc 2004;228:620–34.
[66] Cheglokov AE, Ulenikov ON, Zhilyakov AS, Cherepanov VN, Makushkin YuS, Malikova AB. On the determination of spectroscopic constants as functions of intramolecular parameters. J Phys B 1989;22:997–1015.
[67] Nielsen HH. The vibration–rotation energies of molecules. Rev Mod Phys 1951;23:90–136.
[68] Watson JKG. Determination of centrifugal distortion coefficients of asymmetric–top molecules. J Chem Phys 1967;46:1935–49.
[69] Papousek D, Aliev MR. Molecular vibrational–rotational spectra. Amsterdam, Oxford, New York: Elsevier Scientific Publishing Company; 1982.
[70] Ulenikov ON, Liu A-W, Bekhtereva ES, Gromova OV, Hao L-Y, Hu SM. High–resolution fourier transform spectrum of H_2S in the region of the second hexade. J Mol Spectrosc 2005;234:270–8.
[71] Ulenikov ON, Bekhtereva ES, Grebneva SV, Hollenstein H, Quack M. High–resolution rovibrational analysis of vibrational states of A_2 symmetry of the dideuterated methane CH_2D_2: the levels ν_5 and $\nu_7 + \nu_9$. Mol Phys 2006;104:3371–86.
[72] Ulenikov ON, Bekhtereva ES, Albert S, Bauerecker S, Hollenstein H, Quack M. High–resolution near infrared spectroscopy and vibrational dynamics of dideuteromethane (CH_2D_2). J Phys Chem A 2009;113:2218–31.
[73] Bykov AD, Makushkin YuS, Ulenikov ON. The vibrational analysis of $H_2^{16}O$. J Mol Spectrosc 1983;99:221–7.
[74] Ulenikov ON, Gromova OV, Bekhtereva ES, Kashirina NV, Maul C, Bauerecker S. Precise ro–vibrational analysis of molecular bands forbidden in absorption: the $\nu_8 + \nu_{10}$ band of $^{13}C_2H_4$. J Quant Spectrosc Radiat Transf 2015;164:117–28.
[75] Zhilinskii BI. Method of irreducible tensorial sets in molecular spectroscopy. Moscow: Moscow State University Press; 1981.
[76] Moret-Bailly J, Gautier L, Montagutelli J. Clebsch–Gordan coefficients adapted to cubic symmetry. J Mol Spectrosc 1965;15:355–77.
[77] Rey M, Boudon V, Wenger Ch, Pierre G, Sartakhov B. Orientation of O(3) and SU(2)⊗C_i representation in cubic point groups (O_h, T_d) for application to molecular spectroscopy. J Mol Spectrosc 2003;219:313–25.
[78] Loëte M. Développement complet du moment dipolaire des molécules tétraédriques. application aux bandes triplement dégénérées et *à* la diade ν_2 et ν_4. Can J Phys 1983;61:1242–59.
[79] Wenger C, Boudon V, Champion JP, Pierre G. Highly–spherical top data system (HTDS) software for spectrum simulation of octahedral XY_6 molecules. J Quant Spectrosc Radiat Transf 2000;66:1–16.

[80] Gromova O.V., Bekhtereva E.S., Raspopova N.I., Kuznetsov A.V., Boudon V., Sydow C., Berezkin K., Bauerecker S. Comprehensive study of the pentad bending triad region of germane: positions, strengths, widths and shifts of lines in the $2\nu_2$, $\nu_2+\nu_4$ and $2\nu_4$ bands of $^{70}GeH_4$, $^{72}GeH_4$, $^{73}GeH_4$, $^{74}GeH_4$, $^{76}GeH_4$. J Quant Spectrosc Radiat Transf 2021, 107526 (https://doi.org/10.1016/j.jqsrt.2021.107526).

[81] Wenger C, Champion JP. Spherical top data system (STDS) software for the simulation of spherical top spectra. J Quant Spectrosc Radiat Transf 1998;59:471–80.

[82] Wenger C, Boudon V, Rotger M, Sanzharov JP, Champion J-P. XTDS and SPVIEW: graphical tools for the analysis and simulation of high–resolution molecular spectra. J Mol Spectrosc 2008;251:102–13.